JPE 18-2-24

https://doi.org/10.6113/JPE.2018.18.2.588
ISSN(Print): 1598-2092 / ISSN(Online): 2093-4718

Power Flow Control at the Subnetwork-Level in Microgrids

Kun Liu[†], Muhammad Mansoor Khan[*], Ahmad Rana[**], and Dong Fei[***]

[†,*]Department of Electrical Engineering, Shanghai Jiao Tong University, Shanghai, China
[**]Department of Mechanical Engineering, Villanova University, Villanova, PA, USA
[***]State Grid Shanghai Procurement Company, Shanghai, China

Abstract

This paper presents the idea of a smart load that can adjust the input power flow based on the intermittent power available from RESs (Renewable Energy Resources) to regulate the line voltage, and draw a constant power from the grid. To this effect, an innovative power flow controller is presented based on a Resistive ES (Electric Spring) in combination with a PEAT (Power Electronics based Adjustable Transformer), which can effectively shape the load power flow at the subnetwork level. With a PEAT incorporated in the step down transformer at the grid side, the proposed controller can supply non-critical loads through local RESs, and the critical loads can draw a relatively constant power from the grid. If there is an abundance of power produced by the RESs, the controller can supply both non-critical loads and critical loads through the RES, which significantly reduces the power demand from the grid. The principle, practicality, stability analysis, and controller design are presented. In addition, simulation results show that the power flow controller performs well in shaping the load power flow at the subnetwork level, which decreases the power demand on the grid. Experimental results are also provided to show that the controller can be realized.

Key words: Electric spring, microgrid, Power electronics based adjustable transformer, Power flow control, Renewable energy sources

I. INTRODUCTION

Electrical power generation using non-fossil fuel RESs has received a lot of interest in recent years. However, one of the active areas of research is mitigating the impact of the intermittent nature of RESs on the grid. These fluctuations in energy generation, when added to fluctuation of the load demand on the distribution side, lead to instabilities in the grid [1]. Conventional techniques, such as droop control, exist for voltage regulation due to fluctuations in demand. However, due to line impedance imbalances in the grid, conventional droop control cannot achieve power sharing. To improve load sharing accuracy, a high gain angle droop control method can be adopted [2]. However, this is not enough to compensate for added fluctuations due to the intermittent power generation of RESs. The high droop gain results in poor power quality [3], and droop control is no longer sufficient [4]-[6].

The storage of excess energy has been explored in depth in auxiliary storage plants such as batteries [7], [8], fuel cells [9]-[11], superconducting magnetic energy storage [12], [13] and ultra-capacitor energy storage [14]. This excess energy can then be used to compensate for an increase in demand on the load side when the RESs are not able to provide energy due to their intermittent nature. However, this methodology is limited due the costs associated with the available technologies, as well as their environmental impact [15], [16].

In addition to droop control and energy storage on the generation side to mitigate the impact of the energy fluctuations, an alternative is to consider the DR (Demand- Response) by varying the demand based on availability [17], [18]. This has a promising economic feasibility and may play an increasingly important role in the energy efficiency of grid power. Based on the required communication technology, DR implementations can be categorized into communication based load varying methods [19], [20] and direct measurement based load varying

Manuscript received Oct. 6, 2016; accepted Nov. 2, 2017
Recommended for publication by Associate Editor Kyeon Hur.
[†]Corresponding Author: liukunaliukun@163.com
Tel: +86-13681668949, Shanghai Jiao Tong University
[*]Dept. of Electrical Eng., Shanghai Jiao Tong University, China
[**]Mechanical Eng. Department, Villanova University, USA
[***]State Grid Shanghai Procurement Company, China

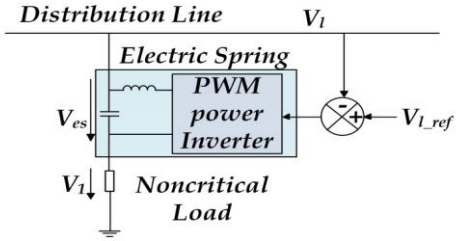

Fig. 1. Electric Spring.

methods. For the former, the performance depends on reliable, highly efficient and secure communication which requires a complex and expensive infrastructure. The latter only requires a sparse communication network, e.g. ES (Electric Spring) [21]~[29], that adopts the demand side management control method where the load demand follows the power generation. Electric Spring uses a principle analogous to Hooke's law for a 'mechanical spring' in the electric regime. Just as a mechanical spring system that is able to: i) provide mechanical support, ii) store mechanical energy, and iii) dampen mechanical oscillations; an ES can: i) provide electric voltage support, ii) store electric energy, and iii) dampen electric oscillations [23]. Fig. 1 shows one kind of ES topology and its control scheme. The error of the line voltage V_l and the reference voltage V_{l_ref} is fed to the PWM power inverter controller to regulate the ES output voltage V_{es}, in an effort to maintain V_l at its normal value. When V_l is lower than V_{l_ref}, V_{es} increases to keep V_l equal to V_{l_ref} and vice versa. The ES and the non-critical load (voltage insensitive, such as a water heater) that it controls form a smart load [22] that can adaptively consume power according to the available intermittent power generation. However, the study of ES is relatively new, and many of its application issues have not been addressed yet. In present studies, an ES is used as a local control that can regulate the voltage and power at the device-level. However, it cannot shape the available power from the generation side. This may lead to improper power distribution at the subnetwork level.

This paper augments research on the ES and proposes a method for power flow control based on a resistive ES and a PEAT. The PEAT acts as a power flow controller that can shape the available power generation provided for a subnetwork by embedding it in a step down transformer [30]-[32]. The power flow controller, which only needs a sparse communication network, can be designed to shift most of the RES fluctuating power to non-critical loads (such as air conditioners, heater units or mobile electric vehicle battery chargers, where a slight delay in the availability of power does not impact operation, which means that power scheduling is possible). As a result, non-critical loads can be powered by local RESs, or by excess power from the main grid. The critical loads (such as lights and computers), which are voltage sensitive and need to be on when required, are mainly powered by the grid. If there is an abundance of power being produced by RESs, the controller can supply both non-critical loads and critical loads through RESs, which significantly reduces the power demand for the grid. This is a promising way to ease the tension of a grid power supply to meet sudden and rapid increases of electricity demand, or when the supply of energy from RESs suddenly drops due to their intermittent nature. This proposed method broadens the application scope of ES based systems by utilizing them in shaping the power flow at the subnetwork level.

This paper is organized as follows. Section II introduces the ES+PEAT based power flow system. Section III discusses the practicality of this new methodology. Section IV provides a system stability analysis. Section V presents the structure and design of an innovative dual mode power flow controller. Section VI shows the effectiveness of the proposed system through an extensive simulation study. An experimental setup is built and results from this experimental setup are provided in Section VII. Finally, Section VIII provides conclusions derived from the analysis, simulation studies and experimental results.

II. Principles of a Resistive ES based Power Flow Controller

In the proposed method, a PEAT is added to a network in combination with a Resistive ES to form a power flow controller. The combination of the global control of a PEAT and the local control of a resistive ES makes it possible to effectively shape the power flow at the subnetwork level with simultaneous stabilization of the fluctuating line voltage. The design principle of a PEAT is similar to that of the Power Flow Controller (PFC) proposed by Majumder et al. [33]. However, unlike the PFC, a PEAT only modifies the in-phase voltage at the output, and basically forms an electronic version of a tap-changer [34]-[38]. The component cost of a PEAT is lower than that of a PFC since it can be directly designed using AC/AC converters (details can be found in [39], [40]), which are compact in design and suffer from lower dissipation losses. Fig. 2(a) shows one type of AC/AC converter with a full-bridge 8-switch topology with key waveforms, where V_i and V_o are the input voltage and the output voltage, respectively. The switches S1~S4 convert full wave line voltages to half wave line voltages, and the switches S5~S8, modulated with a constant duty cycle, convert this signal back to a full wave signal. The magnitude of the output voltage can be modified by changing the duty cycle at the switches S5~S8. In the conventional design, AC/AC converters are used in combination with a buck-boost transformer to form an electronic version of a tap changer as shown in Fig. 2(b). This sort of implementation of a PEAT is not feasible for its application in a Microgrid because of its high cost. To make it more cost effective and feasible for

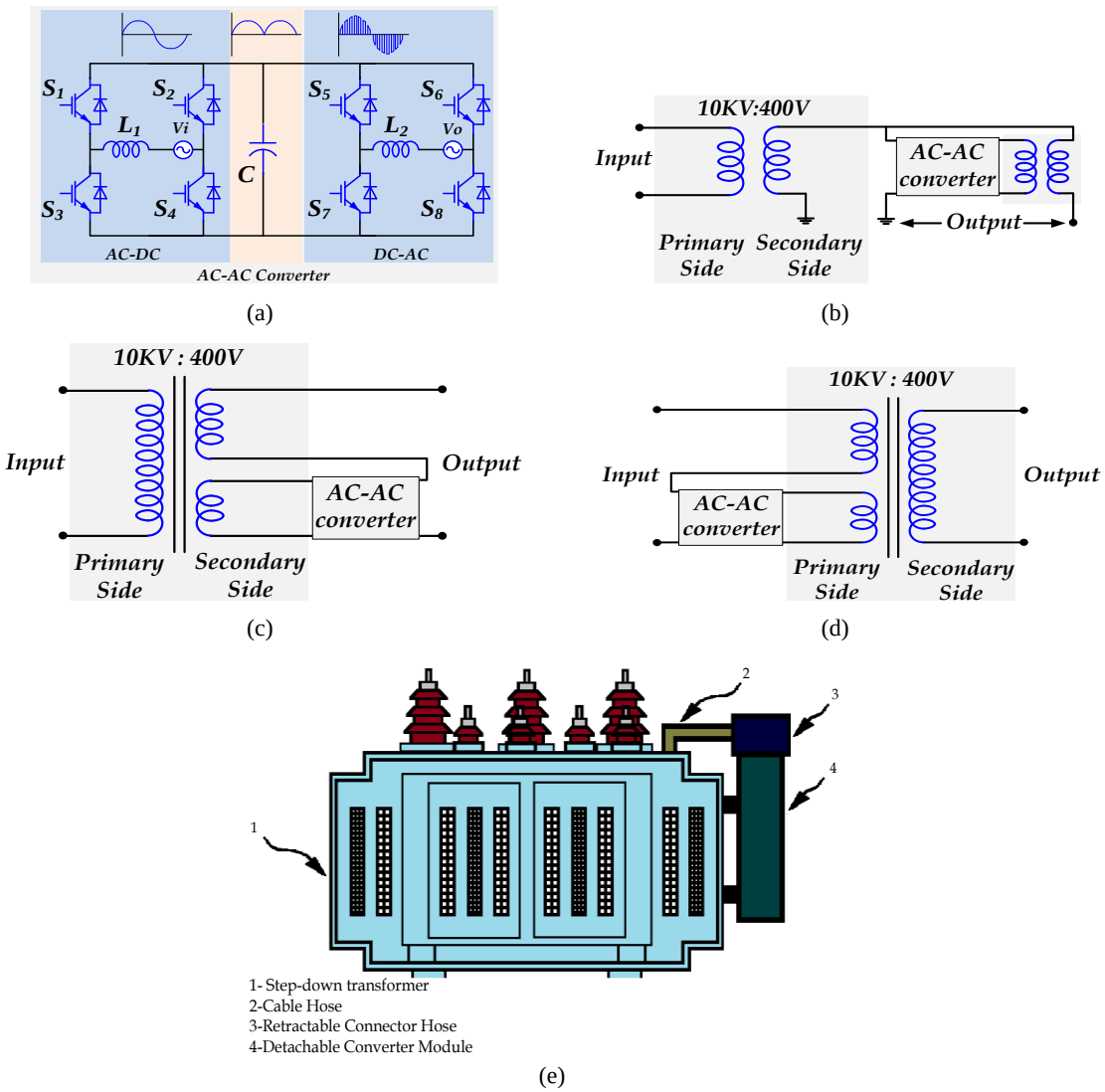

Fig. 2. (a) Single phase full bridge AC/AC converter. (b) PEAT topology with a buck/boost transformer. (c) Modified PEAT design for integration with a step down transformer, and an AC/AC module installed at secondary side. (d) Modified PEAT design for integration with a step down transformer, and an AC/AC module installed at the primary side. (e) PEAT physical construction.

Microgrid applications, the integrated design of a PEAT at the utility-side 10KV/400V step-down transformer is proposed. Two possible implementations of such a combination are considered here. The first is to implement an AC/AC converter based tap-changer at the secondary side [Fig. 2 (c)], which is usually 400Vac. Instead of installing a separate buck-boost transformer in this configuration, an additional winding fraction of the secondary side is added to the existing step down transformer. The voltages from this winding are added to the output voltages using a bidirectional AC/AC converter to modify the output voltages. This sort of PEAT design requires a lower voltage, but higher current rating switching devices, since the secondary side of the step down transformer is generally highly dependent on the power rating of the transformer. The second way is to implement the PEAT on the primary side of the 10KV transformer using an AC/AC converter [Fig. 2 (d)]. This method results in lower conduction losses in the AC/AC converter. Hence, it is more feasible in practical designs. Fig. 2 (e) shows the practical construction of the proposed PEAT design, where a detachable converter module is embedded into the step down transformer through a retractable connector hose and a cable hose.

The detachable converter module can be removed or installed conveniently according to the usage requirements and for maintenance purposes. In the absence of an AC/AC converter the transformer can work as a conventional step down transformer with automatic bypass switches installed in the connector hose. The detailed implementation of a PEAT will be reported in a future research.

The power flow control consists of two control levels. The global control is designed to control the RES power and grid

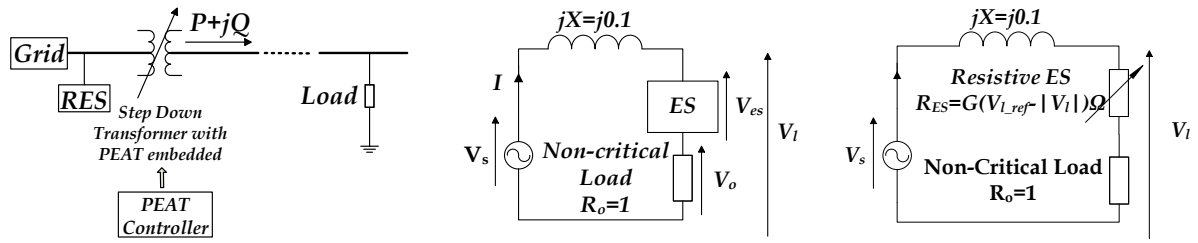

(a) (b) (c)

Fig. 3. (a) Simplified network with a PEAT; (b) inductive ES control method; (c) resistive ES control method.

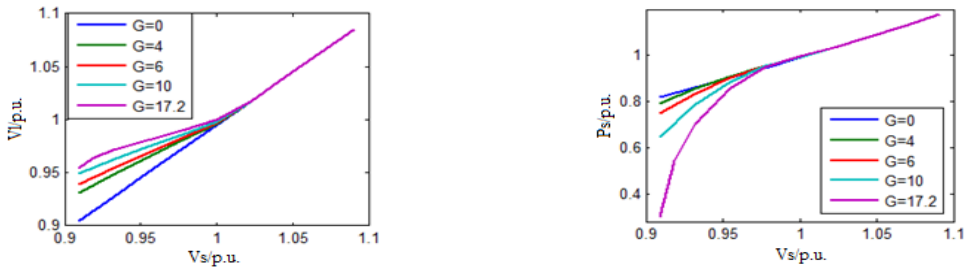

(a) (b)

Fig. 4. (a) Line voltage V_l curve when the source voltage V_s changes ±10% by applying the inductive ES method; (b) active power P_s curve when the source voltage V_s changes ±10% by applying the inductive ES method.

power supply at the generation side by changing the duty cycle of the AC/AC converter. The local control regulates the power flow at the device level using an ES. In the simple system shown in Fig. 3(a), the power can be supplied through a PEAT, which can be designed to modify the line voltage to be within a range of 220V±5%. Then, the ES method is applied to modify the power of non-critical loads and to keep the power of critical loads stable. This section studies two kinds of load varying methods in combination with a PEAT: the inductive ES method and the resistive ES method.

Simplified single phase system diagrams are given in Fig. 3(b) and (c) for the inductive ES and resistive ES, respectively. The grid side voltage at the output of the PEAT can be approximated by an adjustable voltage source V_s with a series impedance jX.

The inductive ES is analyzed first. The load power fluctuates with variations in the line voltage. In residential distribution network systems, such as heating/cooling units, can be considered as non-critical load [22]. V_{l_ref} is the nominal voltage reference and V_l is the load terminal voltage (Fig. 3 (c)). The ES device measures the voltage V_{es} at its terminal and adjusts its impedance accordingly. Considering the cost factor in ES implementations, the use of a battery [15] is ruled out, and it is replaced with a capacitor. For the different values of gain G in Fig. 3(b), the magnitude of the ES voltage can be given as:

$$|V_{es}| = G(V_{l\_ref} - |V_l|). \quad (1)$$

V_{es} should be in quadrature with its current since the power dissipation in the ES is zero. Furthermore, to protect the load from over power, the ES is only allowed to shed load. When the PEAT output voltage exceeds the reference voltage, the ES is deactivated and the load is directly connected to the line.

An example is considered where the line inductance X=0.1pu, the non-critical load resistance is 1pu, V_{l_ref} is 1pu, and V_s is changes from 0.9pu to 1.1pu. The line voltage V_l and active power P_s based on different values of the gain G (0, 4, 6, 10, 17.2) are shown in Fig. 4.

From Fig. 4 it can be observed that the ES can increase V_l, and decrease the active power by injecting voltage V_{es}. When G is larger, the line voltage V_l is increased and the active power P_s is reduced. When the source voltage V_s is around unity pu, the voltage increases and active power reduction is not significant. However, when the source voltage is lower than 0.95pu, the ES can regulate the voltage and power. This is due to voltage restoration capability of the traditional ES [21]-[23]. Hence, the conventional ES does not form a very efficient power flow controller in combination with a PEAT. However, it may be suitable to use an inductive ES in situations where the load is located far from the distribution transformer.

Next, a resistive ES is considered. The resistance of a non-critical load is 1pu, and the controlled load resistance value can be given by following equation $R_{ES} = G(V_{l\_ref}-|V_l|)$, where G is the gain of the ES. The total load impedance is:

$$R = 1 + G(V_{l\_ref} - |V_l|). \quad (2)$$

The line voltage and active power in the resistive ES method can be represented by the following equations:

$$|V_l| = V_s R / \sqrt{R^2 + X^2}, \quad (3)$$

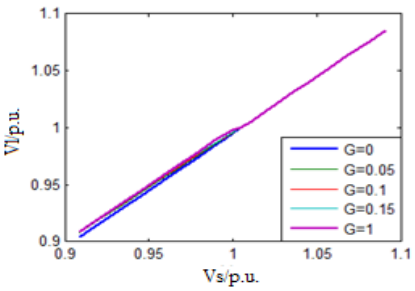

(a)

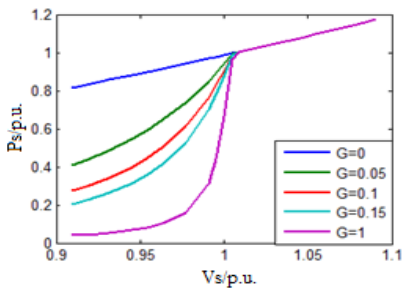

(b)

Fig. 5. (a) Line voltage V_l curve when the source voltage V_s changes ±10% by applying the resistive ES method; (b) active power P_s curve when source voltage V_s changes ±10% by applying the resistive ES method.

$$P_s = V_s^2 R / (R^2 + X^2). \tag{4}$$

Here, the line inductance is X=0.1pu, the reference voltage V_{l_ref} is once again 1pu, and the controlled voltage V_s changes from 0.9pu to 1.1pu. The line voltage V_l and the active power P_s based on different values of the gain G (0, 0.05, 0.1, 0.15, 1) are shown in Fig. 5. The line voltage V_l is increased slightly and P_s is significantly reduced when V_s is lower than the reference voltage. In addition, the larger the value of G, the larger the reduction in power becomes. Take V_s of 0.95 pu as an example. When G is 0.1, the active power P_s is 0.4 pu; and when G is 1, P_s is only 0.07 pu. It can be observed that the active power reduction is significant for the resistive ES method even when V_s is around unity and it only slightly modifies line voltage.

It is evident from Fig. 5 that the consumed power can be adjusted by slight modifications of the PEAT voltages. Hence, this combination of a resistive ES and a PEAT can be effectively exploited to shape the power in the subnetwork.

III. Practicality of a Resistive ES and a PEAT

In the conventional approach to power management, the power utility company is solely responsible for the delivery, quality and cost of the electric supply, depending upon user demand. The concept of the resistive ES+PEAT based control is different from that of the conventional approach. In this approach, the supplier and the consumer are supposed to participate in the utilization of the supply in order to minimize the losses and the costs of generation and transmission. The concept of a smart load has been discussed in renewable based systems [21]-[29]. However, since this is a new methodology, it is necessary to discuss the feasibility of the proposed method. A short discussion of the following attributes of the proposed method has been provided in this section.

- Power Quality on the grid when the resistive ES+PEAT are inserted into the system.
- Suitability of the proposed methodology for different types of residential loads.
- The costs associated with the proposed methodology.

The voltage standard for a critical load is specified in term of voltage quality. It is described in terms of a voltage regulation that should be within a ±5% range of the nominal value voltage flicker, which depends on fast fluctuations of the voltages and voltage distortions. Voltage distortion is measured as the total harmonic distortion, and is supposed to be less than 5%. Since the PEAT does not add any distortion to the voltage, it is not discussed any further. In the subsequent section, a PEAT based control system will be designed in such a manner that it will always keep voltages within the bound of ±5%. When input voltage varies beyond this range, the PEAT works as voltage regulator rather than acting as a power flow controller. However, the smart load responds according to the voltage level and decreases the power absorption if the voltages are lower than the nominal value. As a result, it acts to minimize variations. Hence, the insertion of an ES+PEAT keeps the voltage regulation within the required bounds. However, the insertion of a PEAT results in a flicker in utility voltages. The impact of the flicker depends upon the behavior and variation in power generation intermittency response. Considering the proposed control of the ES+PEAT, it can be seen from Fig. 9 that actual voltage ripple after the insertion of a PEAT is less than 2% which is well within the flicker standards set by [43], [44].

To discuss the suitability of the proposed methodology, two aspects need to be considered.

i. The effects of the insertion of an ES+PEAT on the power quality of critical loads.
ii. The selection and/or modification of the non-critical loads to be used in the methodology.

As discussed in the paragraph above, the insertion of an ES+PEAT in a system does not impact the power quality of critical loads. However, one particular type of load commonly used in utility grids warrants specific mention. This is direct driven motors load like water pumps. The active power transfer in these loads is sensitive to the phase angle between the input and the internal voltage of an electric machine. These loads are more sensitive to variations in the quadrature voltage component of the line voltages when compared to the in-phase component. The PEAT only modifies the in phase component which will results in a slight change in the reactive power of the motor. Once again, the PEAT is designed to

produce fluctuations within ±5% of the nominal value. No significant power level variations are expected in the induction motor or the synchronous motor loads.

The selection of non-critical loads is another very important aspect for the suitability of the proposed methodology. If certain loads cannot be directly used as non-critical loads, then a path to the modification of these loads should exist. These modifications, if cost effective, should make them suitable for use as non-critical loads. Different types of residential loads, such as battery chargers and environment control units like air-conditioners and heater are discussed here.

Two kinds of intermittent sources, wind power and solar power, and how they can impact the choice of non-critical loads, are considered in this section. In the case of wind power, the fluctuation in energy can vary in second to hour range [45]. Hence, the lower bound for fluctuations ranges in seconds. Therefore, for reasonable design, a smart load with a response time of less than a second would be enough to divert most of the wind power fluctuation of the load. In the case of solar energy production, the fluctuations are relatively fast and occur in range of a few hundred milliseconds. Here, a more elaborate design is required, where super capacitors in combination with a PEAT can be used to effectively deal with the fast power fluctuations. This is currently being investigated, and will be the subject of future publications.

Battery chargers can be converted into smart loads. Battery chargers are designed with ±10% to a 15 percent input range. At the input stage of these units, a power factor correction rectifier or a three phase bidirectional converter is used. These systems have dynamic responses in tens of milliseconds. In this way, they can easily be transformed to be used with an ES with added control methods, which provides control for the required response time.

Environment control systems form a very large proportion of residential loads. These can be transformed to a resistive ES by designing systems with a reasonable capacity to store direct or indirect forms of heating / cooling, which can be utilized according to consumer demand throughout the day. For heating systems, one option is to store the heat in water which circulates in a home through heat radiators. The energy stored in the water is supplied by an ES system. Similarly, conventional inverter driven air conditioning units can be adapted for the proposed resistive ES, and the power variations in these system can be accomplished through speed variation and cooling throttle control, which are well established technologies. Storage in chilled water can be adapted for these systems, which is already used in the cooling system of large buildings. Another way to form an air-conditioning system suitable for a resistive ES is to use a desiccant based air conditioning system. These kinds of air-conditioning systems are becoming increasingly available for renewable option since they can run directly on heat and indirectly store cooling in the form of desiccant. Several thermodynamic cycles and practical methods are available for desiccant based air-conditioning. However, they are beyond the scope of this paper. Since these systems can run directly on the heat produced by electricity or a combination of heat sources, they form a perfect candidate for an ES. The details of the ES design will be the subject of a future publication.

Finally, a discussion about the cost of the proposed solution is in order. In distributed generation using renewable energy resources, intermittency is a major issue. This is normally dealt with by using expensive battery storage systems. In the case of residential power conversion, these systems require electric energy to go through a double conversion loss before being utilized in applications such as heating or cooling. The major task of an ES+PEAT system is to minimize this storage system by intelligently utilizing an intermittent form of energy production to minimize the cost and losses associated with these storage systems.

Some of the methods of energy storage for environmental control systems have been discussed in the paragraphs above. The energy storage in the ES is more effective than battery storage systems since no expensive materials or construction techniques are required. There are no additional costs associated with a suitable heating system for the proposed ES, but the initial costs of the ES based air-conditioning system are higher than conventional air-conditioning systems. In the long run, these costs can be offset by the lower production cost based metering of electricity, since they have an unlimited life span when compared to alternative systems using batteries.

IV. Stability Analysis

In order to analyze the system stability, a simplified system composed of a voltage recourse V_s, an Electric Spring V_{es}, and a line impedance L is considered.

As shown in Fig. 6, V_l is the line voltage, and I_1, I_2 and I_3 are the current flows through the non-critical load R_1, critical load R_2 and transmission line, respectively.

In the time domain, the following is obtained:

$$V_{sabc} - V_{labc} = L\frac{dI_{3abc}}{dt}. \tag{5}$$

Applying inverse PARK Transform yields:

$$C^{-1}V_{sdq0} - C^{-1}V_{ldq0} = L\frac{d(C^{-1}I_{3dq0})}{dt}. \tag{6}$$

From equation (6), it is possible to obtain:

$$C^{-1}V_{sdq0} - C^{-1}V_{ldq0} = L\frac{dC^{-1}}{dt}I_{3dq0} + LC^{-1}\frac{dI_{3dq0}}{dt}. \tag{7}$$

Multiplying C in equation (7) on both sides yields:

$$\begin{bmatrix} V_{sd} \\ V_{sq} \end{bmatrix} - \begin{bmatrix} V_{ld} \\ V_{lq} \end{bmatrix} = L\begin{bmatrix} 0 & -w \\ w & 0 \end{bmatrix}\begin{bmatrix} I_{3d} \\ I_{3q} \end{bmatrix} + L\begin{bmatrix} \dot{I}_{3d} \\ \dot{I}_{3q} \end{bmatrix} \tag{8}$$

From the system block it is possible to obtain:

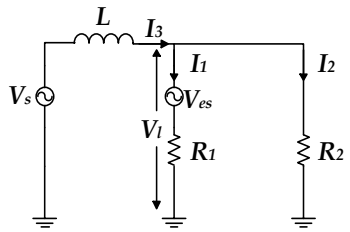

Fig. 6. Simplified system.

$$\begin{bmatrix} V_{ld} \\ V_{lq} \end{bmatrix} = \frac{R_2}{R_1+R_2}\begin{bmatrix} V_{esd} \\ V_{esq} \end{bmatrix} + \frac{R_1R_2}{R_1+R_2}\begin{bmatrix} I_{3d} \\ I_{3q} \end{bmatrix}. \quad (9)$$

For an Electric Spring, the controller compares the line voltage magnitude $|V_l|$ with the reference peak voltage 311V (the corresponding RMS value is 220V), the error is multiplied by the gain k_{es} to get the voltage magnitude of the Electric Spring, and it is in phase with the current I_2 which flows through the load R_1. In this case, V_{es} is in phase with I_1. Therefore, I_1, I_2 and I_3 are all in the same phase. In order to simplify the equations, I_3 is used to replace I_2 in the ES equation, which implies that:

$$V_{es} = kes(311 - |V_l|)\frac{I_3}{|I_3|} \quad (10)$$

In the dq0 form:

$$V_{esd} + jV_{esq} = kes(311 - \sqrt{V_{ld}^2 + V_{lq}^2})\frac{I_{3d} + jI_{3q}}{\sqrt{I_{3d}^2 + I_{3q}^2}}. \quad (11)$$

Linearize equation (11):

$$\begin{bmatrix} \Delta V_{esd} \\ \Delta V_{esq} \end{bmatrix} = \begin{bmatrix} md & mq \\ mdd & mqq \end{bmatrix}\begin{bmatrix} \Delta I_{3d} \\ \Delta I_{3q} \end{bmatrix} + \begin{bmatrix} nd & nq \\ ndd & nqq \end{bmatrix}\begin{bmatrix} \Delta V_{ld} \\ \Delta V_{lq} \end{bmatrix}. \quad (12)$$

Where the parameters are:

$$md = kes(311 - \sqrt{V_{ld}^2 + V_{lq}^2})\frac{I_{3q}^2}{\left(I_{3d}^2 + I_{3q}^2\right)^{\frac{3}{2}}} \quad (13)$$

$$mq = -kes(311 - \sqrt{V_{ld}^2 + V_{lq}^2})\frac{I_{3d}I_{3q}}{\left(I_{3d}^2 + I_{3q}^2\right)^{\frac{3}{2}}} \quad (14)$$

$$mdd = -kes(311 - \sqrt{V_{ld}^2 + V_{lq}^2})\frac{I_{3d}I_{3q}}{\left(I_{3d}^2 + I_{3q}^2\right)^{\frac{3}{2}}} \quad (15)$$

$$mqq = kes(311 - \sqrt{V_{ld}^2 + V_{lq}^2})\frac{I_{3d}^2}{\left(I_{3d}^2 + I_{3q}^2\right)^{\frac{3}{2}}} \quad (16)$$

$$nd = \frac{-kesI_{3d}V_{ld}}{\sqrt{I_{3d}^2 + I_{3q}^2}\sqrt{V_{ld}^2 + V_{lq}^2}} \quad (17)$$

$$nq = \frac{-kesI_{3d}V_{lq}}{\sqrt{I_{3d}^2 + I_{3q}^2}\sqrt{V_{ld}^2 + V_{lq}^2}} \quad (18)$$

$$ndd = \frac{-kesI_{3q}V_{ld}}{\sqrt{I_{3d}^2 + I_{3q}^2}\sqrt{V_{ld}^2 + V_{lq}^2}} \quad (19)$$

$$nqq = \frac{-kesI_{3q}V_{lq}}{\sqrt{I_{3d}^2 + I_{3q}^2}\sqrt{V_{ld}^2 + V_{lq}^2}}. \quad (20)$$

Substituting the linearized form of equation (9) into (12) results in:

$$\begin{bmatrix} \Delta V_{esd} \\ \Delta V_{esq} \end{bmatrix} = \begin{bmatrix} 1 - \frac{R_2nd}{R_1+R_2} & -\frac{R_2nq}{R_1+R_2} \\ -\frac{R_2ndd}{R_1+R_2} & 1 - \frac{R_2nqq}{R_1+R_2} \end{bmatrix}^{-1}\begin{bmatrix} md + \frac{R_1R_2nd}{R_1+R_2} & mq + \frac{R_1R_2nq}{R_1+R_2} \\ mdd + \frac{R_1R_2ndd}{R_1+R_2} & mqq + \frac{R_1R_2nqq}{R_1+R_2} \end{bmatrix}\begin{bmatrix} \Delta I_{3d} \\ \Delta I_{3q} \end{bmatrix} \quad (21)$$
$$\begin{bmatrix} \Delta V_{esd} \\ \Delta V_{esq} \end{bmatrix} = M^{-1}S\begin{bmatrix} \Delta I_{3d} \\ \Delta I_{3q} \end{bmatrix}.$$

Substituting the linearized form of equations (9) and (21) into the linearized form of equation (8) yields:

$$\begin{bmatrix} \Delta \dot{I}_{3d} \\ \Delta \dot{I}_{3q} \end{bmatrix} = -\frac{1}{L}\left(\frac{R_2}{R_1+R_2}M^{-1}S + W\right)\begin{bmatrix} \Delta I_{3d} \\ \Delta I_{3q} \end{bmatrix} + \frac{1}{L}\begin{bmatrix} \Delta V_{sd} \\ \Delta V_{sq} \end{bmatrix} \quad (22)$$
$$\begin{bmatrix} \Delta \dot{I}_{3d} \\ \Delta \dot{I}_{3q} \end{bmatrix} = A\begin{bmatrix} \Delta I_{3d} \\ \Delta I_{3q} \end{bmatrix} + B\begin{bmatrix} \Delta V_{sd} \\ \Delta V_{sq} \end{bmatrix}.$$

where:

$$W = \begin{bmatrix} \frac{R_1R_2}{R_1+R_2} & -Lw \\ Lw & \frac{R_1R_2}{R_1+R_2} \end{bmatrix} \quad (23)$$

The Eigen values of matrix A show the stability of the system. Test results are shown in TABLE I of the Appendix, under a poor subnetwork condition. The RMS value of V_s is the lowest output voltage of the PEAT embedded in the step down transformer 210V. The transmission line inductance L is 3.1381e-4 H. The heavy non-critical and critical loads both have a rated power of 48.4kW. Here, λ_1 and λ_2 are the Eigen values of matrix A.

As shown in TABLE I, the ES voltage V_{es} increases as the gain G increases. In addition, when G is large enough, V_{es} exceeds the line voltage V_l and the non-critical load voltage V_1 is negative, e.g. when G is 20 and 30. The system is stable since all of the Eigen values are in left-half plane.

V. Power Flow Control Strategy and Controller Design

A PEAT in combination with a resistive ES can be utilized in a number of ways to control power at the subnetwork level. In order to demonstrate the functionality of the proposed power flow control method both for shaping the available power and for stabilizing the critical load power, the setup shown in Fig. 7 is considered. MATLAB/SIMULINK [41] is used to simulate this setup. The utility grid side power source is approximated by an ideal AC Voltage source. The wind power is created using the Wind Turbine Induction Generator

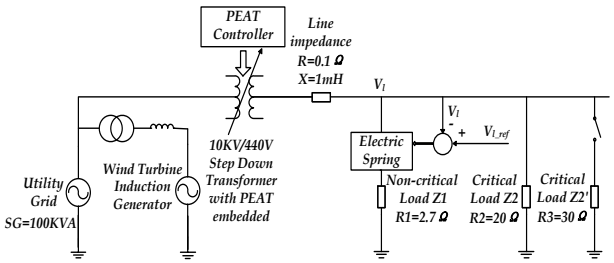

Fig. 7. A simplified power network with both ES and PEAT.

(Phasor Type) block from the Renewable Energy Systems blocks in Mathworks' Simscape Power Systems.

For the network shown in Fig. 7, there are two different cases that are considered to highlight the control strategy. The objective of the first case is to demonstrate the power flow function to shift most of the wind power to a non-critical load to minimize the impact of its intermittent availability on the network. The objective of the second case is to demonstrate the power flow function to decrease the total load demand on the grid. The critical load and the non-critical load are controlled to be mostly supplied locally by the RES, which minimizes the use of grid power for the entire subnetwork. For the sake of simplicity, the loads have been lumped into two sets: non-critical load Z_1 and critical load Z_2, as shown in Fig. 7. The grid power is controlled by a PEAT, and the total load power is a function of the PEAT terminal voltage V_{PEAT}, the wind power P_{wind}, and the impedance of the loads Z_1 and Z_2. In addition, the line impedance Z_{line} is represented as:

$$P_{load} = f = f(V_{PEAT}, P_{wind}, Z_1, Z_2, Z_{line}). \quad (24)$$

The line impedance is ideally assumed to be constant. Therefore, from equation (24), the following can be derived:

$$\Delta P_{load} = \frac{\partial f}{\partial V_{PEAT}} \cdot \Delta V_{PEAT} + \frac{\partial f}{\partial P_{wind}} \cdot \Delta P_{wind} + \frac{\partial f}{\partial Z_1} \cdot \Delta Z_1 + \frac{\partial f}{\partial Z_2} \cdot \Delta Z_2. \quad (25)$$

In order to control the critical load power to be stable despite wind power fluctuations $\frac{\partial f}{\partial P_{wind}} \cdot \Delta P_{wind}$, the power flow controller is designed to regulate the grid power flow using a PEAT.

Based on this control strategy, a novel dual mode control structure is designed that works as a power flow controller when the mains voltage is in the normal range within 220V±5%, and as a voltage regulator beyond this range. Fig. 8 shows a block diagram of this controller. The upper part is the voltage range detector to determine whether the line voltage V_l is within the normal range or not. When the line voltage is less than the lower limit value V_{l_down} = 209V or greater than the upper limit value V_{l_up} = 231V, the difference value (x or y) is positive, and either the function result $1\text{-}e^{-kx}$ or $1\text{-}e^{-ky}$ is 1, where k is a large constant 1e5. Hence one of the saturation blocks is 1. As a result, the weight W_2 in Fig. 8 is 1. Otherwise, W_2 is 0. W_2 is subtracted from 1 to get the

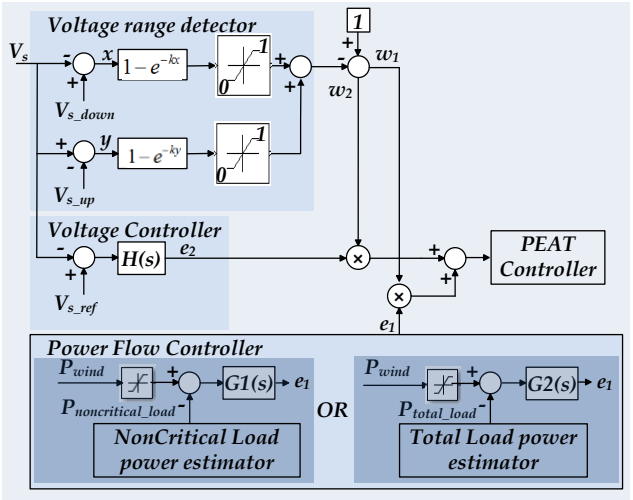

Fig. 8. Dual mode control structure.

complementary value W_1. In this way, W_2 is equal to 1 when the line voltage exceeds the normal range and is equal to 0 when within this range. W_1 is multiplied by the control signal of the power flow controller, and W_2 is multiplied by the voltage controller signal. The dual control mode changes to the power flow control mode when the mains voltage is within the normal range. Otherwise, it changes to the voltage control mode.

Two types of power flow controllers have been designed to achieve two different control objectives. The first power flow controller is used to shift most of the wind power to the non-critical load to reduce the impact of the intermittent power of the RES on the grid. This power flow controller includes a non-critical load power estimator module to obtain the non-critical load power. This module calculates the non-critical load power by applying:

$$P = P_0 + \sum_{i=1}^{N} a_i \Delta V^i. \quad (26)$$

Where P_0 is the power of non-critical load at the normal line voltage 220V, and ΔV is the voltage mismatch of the measured non-critical load voltage and the normal line voltage. The coefficients a_i can be obtained by recursively fitting a polynomial curve to the available data on variations in the power and line voltages. In the presented simulations this has been obtained using the function polyfit in MATLAB.

The difference of the non-critical load power and the wind power is fed to a PI controller *G1* (kp =5e-7, ki=4e-6) to obtain the correction term e_1, as shown in the bottom left section of the power flow controller block diagram in Fig. 8. The PI controller is designed to minimize the difference and to converge to zero. As a result, P_{wind} and $P_{noncritical\_load}$ are balanced. To take into account the maximum power constraint of non-critical loads, a saturation block with the value of $P_{noncritical\_load\_max}$ is added after the wind power.

The second power flow controller decreases the demand

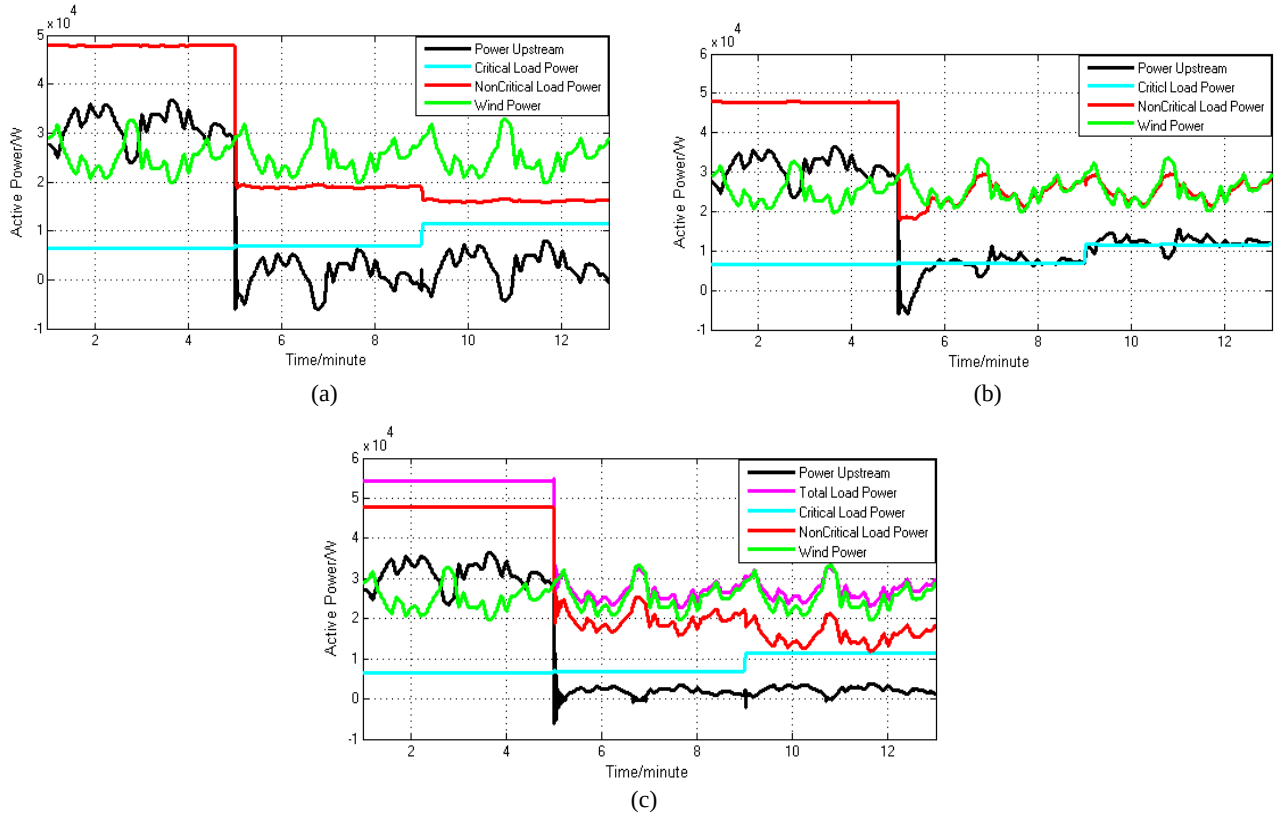

Fig. 9. Active power curves for the simulations: (a) only the ES is applied; (b) both the ES and the PEAT are applied, the first power flow controller is activated; (c) both the ES and the PEAT are applied, the second power flow controller is activated.

for grid power. Since the total load power is mostly supplied locally by wind power, the mismatch of P_{wind} and P_{total_load} obtained from the total load power estimator module can be used to obtain the correction term e_1, as shown in the right bottom section of the power flow controller block diagram in Fig. 8. This module calculates the total load power in a similar way as the non-critical load power estimator module. The function of the PI controller *G2* (kp =4e-6, ki=5e-8) is also aimed to minimize the mismatch, and P_{wind} and P_{total_load} are controlled to be balanced. A saturation block is added after the wind power, with the saturation value of the maximum power constraint of the total load $P_{total\_load\_max}$.

The voltage controller detects the voltage downstream of the distribution line. The difference in the line voltage and the reference voltage is then fed to a PI controller *H* (kp =1, ki =80), to get the second correction term e_2. This control loop enhances the control when the line voltage outstrips too much around 220V. The PEAT controller has two inputs which are selected according to the voltage range detector.

VI. Case Studies and Simulations

Three different cases are studied: 1) system with only an ES installed in the power network; 2) system with both an ES and a PEAT installed applying the first power flow controller; 3) system with both an ES and a PEAT installed applying the second power flow controller. The values of the parameters for the control system are given in Fig. 8.

A. Case 1): System with Only an ES Installed in the Power Network

The simulation is divided into three parts. In the first part, the ES is deactivated and fluctuating wind power is supplied to the system for the first 5 minutes. In the second part, the ES is activated at the 5 minutes mark. In the third part, the ES is still working but the critical load increases at the 9 minutes mark. Simulation results are shown in Fig. 9(a) and Fig. 10(a). From the active power curves, the grid power (power upstream) fluctuates opposite the wind power up to the 5 minutes mark, and the critical load works at a low voltage as shown in Fig. 10(a). The power is not sufficient to support both the non-critical load and the critical load. When the ES is activated, the ES and the non-critical load form a smart load. The ES decreases the non-critical load power increases the power available to the critical load. As a result, the mains voltage increases to ensure the critical load performance. When the critical load increases at the 9 minute mark, the grid power does not increase accordingly, and the non-critical load power is further reduced to provide more power to the critical load because the total available power is the same before and after the critical load is increased. The grid power fluctuates significantly even when the ES is activated, which

causes grid stability problems.

B. Case 2): System with Both an ES and a PEAT Installed, Applying the First Power Flow Controller

This simulation is also divided into three parts. The first part is the same as that in case 1). In the second and the third parts, the first power flow controller is applied, and both the ES and PEAT (where only the power flow control loop works) are activated. The results are shown in Fig. 9(b) and Fig. 10(b). The measurements are the same as case 1) for the first part. For the second and third parts, the non-critical load power and wind power are almost balanced. The only exception to this is when the wind power is higher than $P_{noncritical\_load\_max}$ = 30 kW at around 7 and 11 minute marks, and the non-critical load reaches its maximum power constraint. Here, it consumes part of the wind power. The performance indicates that the wind power is mostly shifted to the non-critical load, and that the grid provides a relatively constant power for the critical load. However, there is a major deviation after the 5 minute mark for a short period of time because the controller's response time is not fast enough. Fluctuations of the grid power are reduced significantly when compared with case 1). Thus, the intermittent impact of the RES to the grid is reduced. When the critical load increases at the 9 minute mark, the grid power increases accordingly. This ensures that the power supply for the increased critical load and the wind power are balanced with the non-critical load power at the same time. This controller is useful to reduce the impact of fluctuations from the RES to the utility grid. This novel power flow controller performs well in shaping the grid power to be more constant and in transferring the wind power to the non-critical load.

C. Case 3): System with Both an ES and a PEAT Installed, Applying the Second Power Flow Controller

This simulation is also divided into three parts. The first part is the same as that in case 1). In the second and the third parts, the second power flow controller is activated. The results are shown in Fig. 9(c) and Fig. 10(c). Compared to case 1), the grid power fluctuation is much smaller and it is beneficial to reduce the intermittent impact of the RES to the grid. It can be seen from Fig. 10(c) that the grid power is reduced by almost 75% and 80% when compared with case 2) from the 5 minute mark to the 9 minute mark and from the 9 minute mark to the 13 minute mark, respectively. In this case, the wind power is always less than $P_{total\_load\_max}$= 50 kW, and most of the load demand can be satisfied locally by the RES. The results show that the power flow controller is effective in decreasing the load demand for the grid power.

The results of the upstream power, critical load power, non-critical load power, wind power and critical load voltage for case 1), 2) and 3) are presented in Table II. In case 2), the non-critical load power is almost balanced with the wind power and the critical load power remains almost the same

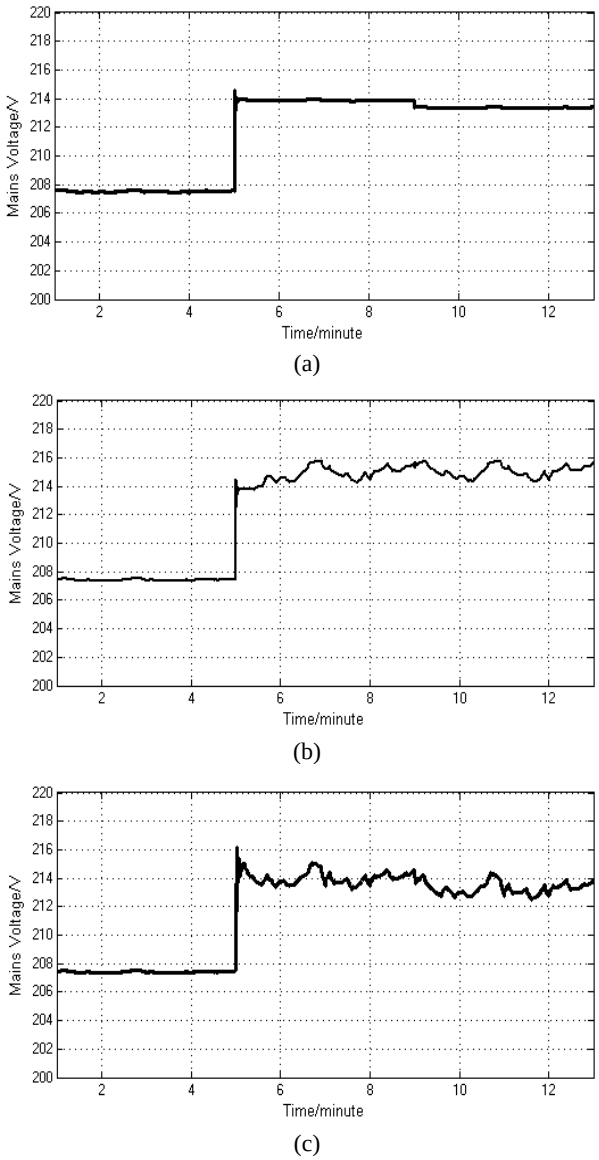

Fig. 10. Mains voltage curves: (a) only an ES is applied; (b) both an ES and a PEAT are applied, the first power flow controller is activated; (c) both an ES and a PEAT are applied, the second power flow controller is activated.

after the 5 minute mark, which indicates that the non-critical loads are supplied locally by the RES and that the critical loads draw a relatively constant power from the grid. The critical load voltage is regulated at around 214.5V and it does not decrease when the critical loads increase in 9 min. In case 3), the upstream power comes down to nearly zero, since most of the critical loads and non-critical loads are supplied by the RES after the 5 minute mark. When the critical loads increase at the 9 minute mark, the non-critical loads power is reduced slightly to shift more power to critical loads, and the critical load voltage also drops slightly because the load demand increases while the RES power does not increase. This verifies the effective performance of the proposed power flow controller.

VII. Practical Experiment Results

Three practical experiments have been set up to evaluate the performance of the proposed power flow controller in this section. a) The first test demonstrates the operation of the PEAT and verifies its ability to vary the voltage and shape the power flow. The input and output voltage waveforms are recorded with different duty cycles. Therefore, the function to vary the voltage of step down transformer and shape the power flow can be examined by changing the duty cycle. b) The second test is the operation of a smart load which consists of an ES and a non-critical load, while an AC/AC buck converter [42] is used to represent the operation of the ES. The setup is shown in Fig. 14. The purpose is to check the ability of the smart load to shed load power when the line voltage drops. c) The third test is to evaluate the function of the proposed power flow controller consisting of a PEAT and an ES in a system as shown in Fig. 17. The system is connected to the grid, and the wind power is simulated by a variable transformer. The performance of the proposed power flow controller is checked by changing the tap changer of the variable transformer to analog the intermittent nature of the wind power.

A. Test a): Operation of a PEAT

The PEAT topology of this test is shown in Fig. 11. The input voltage is applied to an AC/AC converter [39], whose output voltage is varied by changing the duty cycle. Then, the voltage is filtered by a low pass LC filter to make it sinusoidal. The filtered voltage is applied to the compensation transformer and the output voltage of the transformer is added to the PEAT input voltage to get the PEAT output voltage. Fig. 12 shows a practical experiment for the PEAT. The test conditions are V_{in} = 110V (50Hz), and the resistive load is 30.6Ω.

Different duty cycles are applied for the AC/AC converter (0.55 and 0.3). Output voltages of the AC/AC converter before and after the low pass LC filter are measured, shown as $V_{AC/AC}$ and $V_{filtered}$ in Fig. 13. The peak values of $V_{AC/AC}$ are both 155V for different duty cycles, and the peak values of $V_{filtered}$ are 90V and 50V, respectively. The function of the PEAT so that it can change the phase voltage of the step down transformer and shape the power flow by varying the duty cycle of the controller is verified.

B. Test b): Operation of a Smart Load Consisting of an ES and a Non-critical Load

A per-phase schematic of the experiment is illustrated in Fig. 14. An AC/AC buck converter is used to simulate the function of the ES. The line voltage is applied as V_l, and through an AC/AC buck converter whose duty cycle is D and the filter inductance, the desired voltage across the non-critical load R_0 is generated. As shown in Fig. 1, the voltage across the non-critical load R_0 is V_l-V_{es}. Therefore, the duty cycle D can be derived as:

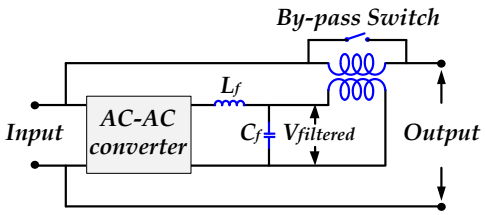

Fig. 11. PEAT topology.

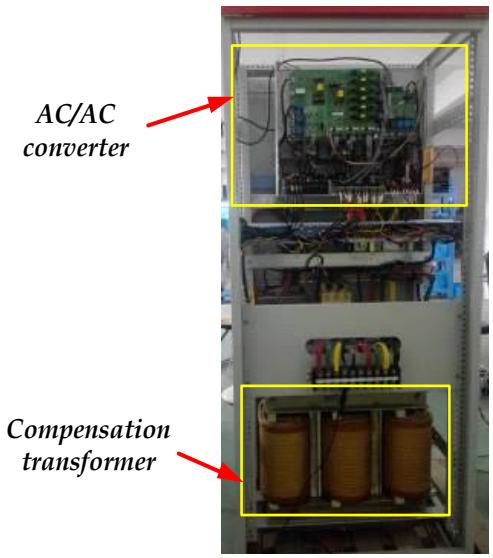

Fig. 12. Photograph of a practical PEAT.

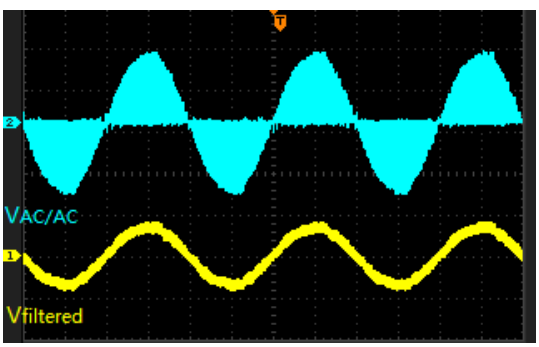

(a)

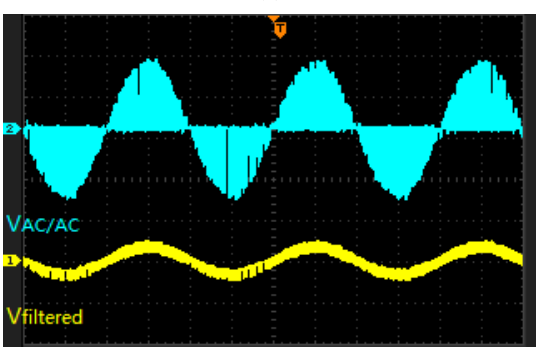

(b)

Fig. 13. Voltage curves of the output voltage of an AC/AC converter before and after applying a low pass LC filter where CH1- $V_{filtered}$, 100V/Div, CH2- $V_{AC/AC}$ 100V/Div, Time Base 5ms/Div: (a) duty cycle is 0.55; (b) duty cycle is 0.3.

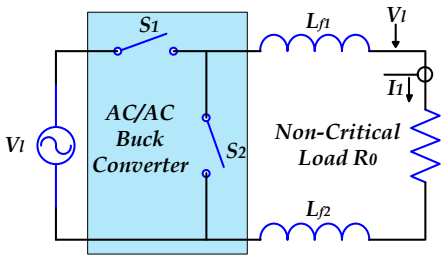

Fig. 14. Topology of an experimental simulation of ES operation.

Fig. 15. Photograph of the AC/AC Buck converter.

$$D = \frac{V_l - V_{es}}{V_l}. \quad (27)$$

Fig. 15 shows a photograph of the practical AC/AC buck converter. The voltage curve and current curve of the non-critical load are measured. R_0 is 30.6 ohm and V_l changes from 310V to 225V at 400ms when the gain of the ES is 0.05. As shown in Fig. 16(a), the current is significantly reduced from 10A to 6A, which implies that the active power is reduced from 1550W to 675W. When the gain of the ES is 0.2, as shown in Fig. 16(b), V_l drops from 310V to 281V at 600ms, and the current drops from 10A to 1.9A. This implies that the active power is shed from 1550W to 267W. This result shows that the resistive ES performs well in shedding power when the mains voltage drops.

C. Test c): Operation of the Proposed Power Flow Controller in a Subnetwork with an Intermittent Wind Power Injection

A subnetwork system is built and the experimental setup schematic is shown in Fig. 17. The system includes a wind power generator, a PEAT, a smart load and a critical load.

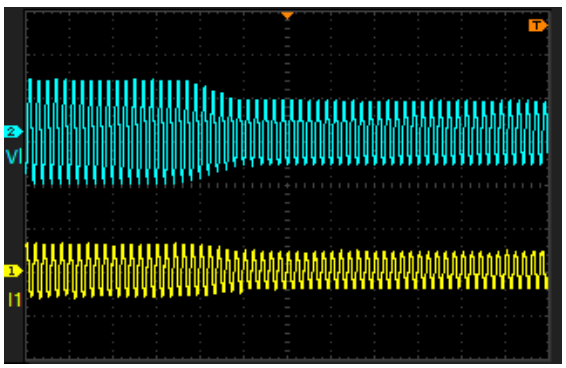

(a)

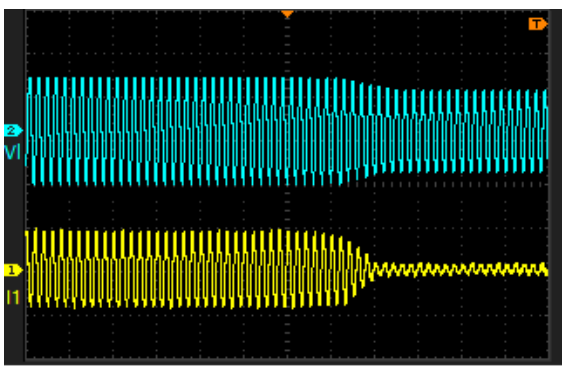

(b)

Fig. 16. Voltage and current curves of a smart load: (a) the ES gain is 0.05, CH1- I_1 15A/Div., CH2- V_l 150V/Div., Time Base 100ms/Div; (b) the ES gain is 0.2, CH1- $I_1$10A/Div., CH2- V_l 150V/Div., Time Base 100ms/Div.

The wind power generator applies a variable transformer to simulate intermittent wind power. The variable transformer varies the voltage by moving the tap changer, and then voltage is applied to the isolation transformer to isolate the voltage from the grid for protection purposes. The isolation transformer output voltage is regulated through a grid connected inverter to simulate intermittent wind power. The PEAT controller regulates the total load power to be balanced with wind power, which is the second power controller in Section V. The smart load automatically sheds the load power. Both the smart load and critical load are connected to the subnetwork. Waveforms of the power source voltage V_s, line voltage V_l, grid current I_1, wind power generator current I_2 and line current I_3 are measured. Fig. 16 shows a photograph of the practical experiment setup. The test conditions are the grid phase voltage V_{grid} = 220Vac, non-critical load Z_1 = 8.2 ohm, critical load Z_2 = 43ohm, G (the gain of the ES) = 31, P (the proportional gain of the power flow controller) = 8 and I (the integral gain of the power flow controller) = 2.

The power flow controller is activated and works throughout the experiment. The purpose of the experiment is to check the performance of power flow controller when wind energy changes. In the beginning, the wind power generator current I_2 is around 3.5A as shown in Fig. 20. It then begins to increase to 28.2A to inject more power into the system, which is

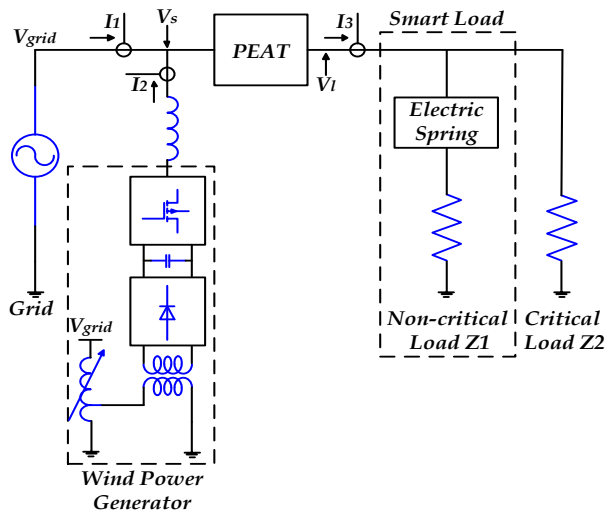

Fig. 17. Experiment setup schematic.

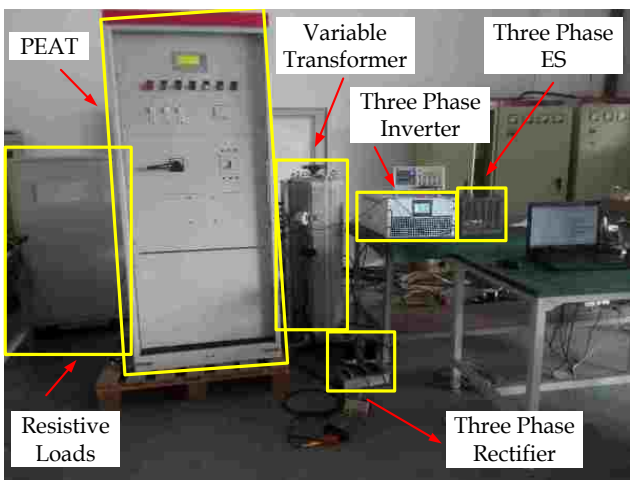

Fig. 18. Photograph of the practical experiment setup.

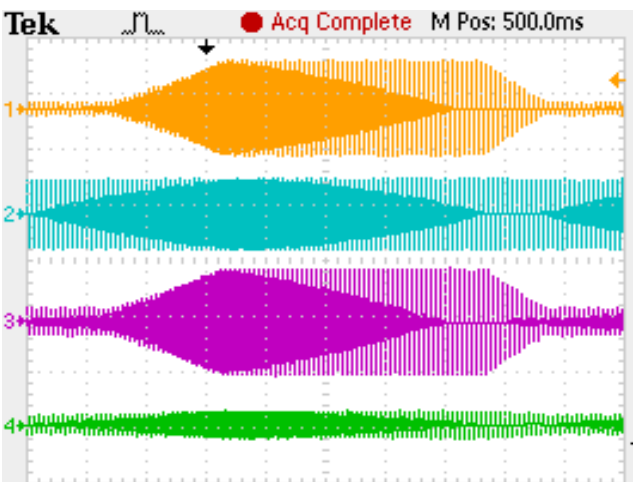

Fig. 19. Measured waveforms where CH1 - wind power generator current I_2 50A/Div., CH2 - Line voltage V_l 500V/Div., CH3 - Line current I_3 50A/Div., CH4 - Grid current I_1 50A/Div., Time Base 250ms/Div.

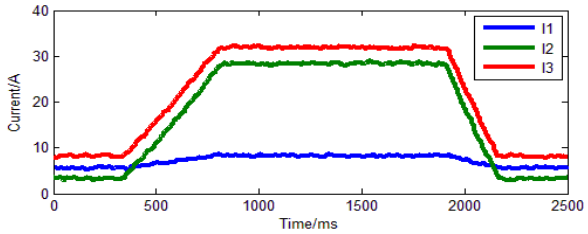

Fig. 20. RMS values of the currents with the grid current I_1, wind power generator current I_2 and line current I_3.

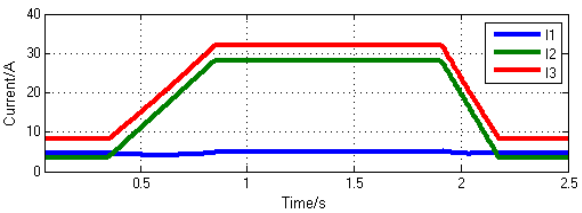

Fig. 21. Simulated RMS values of the currents with the grid current I_1, wind power generator current I_2 and line current I_3.

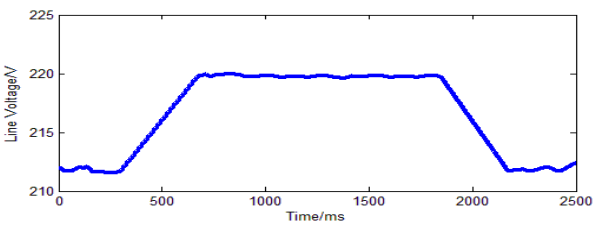

Fig. 22. RMS values of the line voltage.

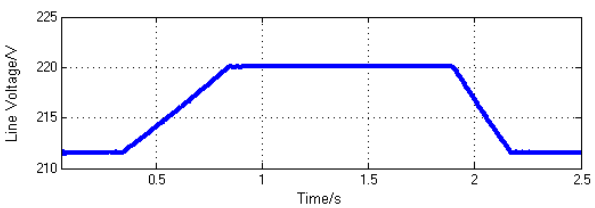

Fig. 23. Simulated RMS values of the line voltage.

simulated in this experiment by changing the tap-changer of the variable transformer of the wind power generator in Fig. 17. The wind power generator current I_2 then decreases to 3.5A again. The experiment result in Fig. 20 show that the line current I_3 increases from 8.2A to 32.0A when the wind power generator injects more power, and decreases to 8.2A when the wind power generator decreases the injected power. This implies that the total load power follows the wind power and that the power flow controller performs well. The grid current only changes slightly when the wind power changes, which shows that the total load power is balanced with the wind power and that the impact of the intermittent nature of the wind power generator on the grid is significantly reduced. Fig. 22 shows that the line voltage is increased by the PEAT and ES of the power flow controller when the wind power increases. As a result, more power is consumed by the load. Fig. 19 shows measured waveforms of the wind power generator

current I_2, line voltage V_l, line current I_3 and grid current I_1. It shows that the line current follows the trend of the wind generator current and that the grid current only changes slightly when the wind generator current changes.

Fig. 21 shows MATLAB simulation results of the RMS values of the grid current I_1, wind power generator current I_2, line current I_3 and line voltage. Comparisons between Fig. 20 and Fig. 21 and between Fig. 22 and Fig. 23 show that the practical experiment results follow the simulation experiment results.

The obtained experiment results validate the function of the proposed power flow controller, which applies the second power controller in Section V. The total load power is balanced with the wind power and the impact of changes in the wind power have a slight impact on grid.

VIII. Conclusions

A novel power flow controller comprising a resistive ES and a PEAT has been developed. The principle behind the control strategy has been described in detail, and a stability analysis performed on the derived mathematical model for the controller shows that it is stable. Simulations carried out for different test cases on this model indicate the effectiveness of the proposed controller in shaping the power flow. An experimental setup is made, and it is shown that the obtained experimental results closely follow the simulation results, indicating that the model of the power flow controller is valid. In addition, the stability analysis and effectiveness of the proposed power flow controller can be extended to actual realization.

The obtained results show that the PEAT plays the role of a global controller and the ES plays the role of a local controller. The combination of these two controllers makes the power flow control complete in terms of controlling the RES power to supply non-critical loads and grid power to supply critical loads. This way, the critical loads, which require a stable and reliable power supply, are guaranteed to be provided with power through the grid, and the non-critical loads can be supplied power through an intermittent but cheaper RES when it is available. If the RES produces abundant power, the critical loads can be supplied power through it instead of the grid.

It can be concluded that the proposed power flow controller is a promising and realizable way to mitigate the effect of the intermittent availability of the RES in the future grid and to ease the tension of the grid power supply to meet sudden changes in electricity demand.

Appendix

TABLE I
System Stability Analysis Test Data

k_{es}	V_l (V)	I_1(A)	I_2(A)	V_{es} (V)	V_1(V)	λ_1	λ_2
0.5	206.0549	199.0824	206.0549	6.9725	199.0824	-1514.8+177.8i	-1514.8-177.8i
1	206.1834	192.3667	206.1834	13.8166	192.3667	-1.1675e3	-1.18626e3
2	206.4274	179.2823	206.4274	27.1452	179.2823	-0.8476e3	-2.3597e3
5	207.0713	142.4275	207.0713	64.6437	142.4275	-0.4773e3	-3.8784e3
10	207.9175	87.0926	207.9175	120.8249	87.0926	-0.2762e3	-7.0481e3
20	209.0533	-9.8798	209.0533	218.9332	-9.8798	-0.0148e3	-1.7656e3
30	209.7082	-99.0452	209.7082	308.7534	-99.0452	-0.0100e3	-4.4733e3

TABLE II
Case Studies Results

		Part1(1~5min)	Part2(6~9min)	Part3(10~13min)
Case 1)	Average Power Upstream(kW)	30.1	0.2	0.2
	Critical load power(kW)	6.5	6.8	11.4
	Non-critical load power(kW)	48.2	19.1	16.0
	Wind power(kW)	25.1	25.1	25.1
	Critical load voltage(V)	207.5	213.8	213.3
Case 2)	Average Power Upstream(kW)	30.1	7.1	11.7
	Critical load power(kW)	6.5	6.9	11.6
	Non-critical load power(kW)	48.2	25.3	25.1
	Wind power(kW)	25.1	25.1	25.1
	Critical load voltage(V)	207.5	214.5	214.6
Case 3)	Average Power Upstream(kW)	30.1	0.2	0.3
	Critical load power(kW)	6.5	6.9	11.4
	Non-critical load power(kW)	48.2	17.9	16.5
	Wind power(kW)	25.1	25.1	25.1
	Critical load voltage(V)	207.5	213.9	213.3

REFERENCES

[1] S. R. Bull, "Renewable energy today and tomorrow," *Proceedings of the IEEE*, Vol. 89, No. 8, pp. 1216-1226, Aug. 2001.

[2] A. Tuladhar, H. Jin, and T. Unger, "Control of parallel inverters in distributed ac power system with consideration of line impedance effect," *IEEE Trans. Ind. Appl.*, Vol. 36, No. 1, pp. 131-138, Feb. 2000.

[3] Z. Liu, "An improved droop control based on complex virtual impedance in medium voltage micro-grid," *IEEE Power and Energy Engineering Conference (APPEEC)*, pp. 1-6, 2013.

[4] F. Shahnia, R. Majumder, and A. Ghosh, "Operation and control of a hybrid microgrid containing unbalanced and nonlinear loads," *Electric Power Systems Research*, Vol. 80, No. 8, pp. 954-965, Aug. 2010.

[5] T. L. Vandoom, J. D. M. De Kooning, and B. Meersman, "Automatic power-sharing modification of P/V droop controllers in low-voltage resistive microgrids," *IEEE Trans. Power Del.*, Vol. 27, No. 4, pp. 2318-2325, Sep. 2012.

[6] R. Majumder, B. Chaudhuri, and A. Ghosh, "Improvement of stability and load sharingin an autonomous microgrid using supplementary droop control loop," *lEEE Trans. Power Syst.*, Vol. 25, No. 2, pp. 796-808, Jul. 2010.

[7] E. Reihani, S. Sepasi, and L. R. Roose, "Energy management at the distribution grid using a battery energy storage system (BESS)," *International Journal of Electrical Power & Energy Systems*, Vol. 77, pp 337-344, May 2016.

[8] A. Subburaj, P. Kondur, and S. B. Bayne, "Analysis and review of grid connected battery in wind applications," *2014 Sixth Annual IEEE Green Technologies Conference*, pp. 1-6, 2014.

[9] B. Shaffer, B. Tarroja, and S. Samuelsen, "Dispatch of fuel cells as transmission integrated grid energy resources to support renewables and reduce emissions," *Applied Energy*, Vol. 148, pp. 178-186, Jun. 2015.

[10] S. Sichilalu, H. Tazvinga, and X. Xia, "Optimal control of a fuel cell/wind/PV/grid hybrid system with thermal heat pump load," *Solar Energy*, Vol. 135, pp. 59-69, Oct. 2016.

[11] W. Chen, Y. Han, and Q. Li, "Design of proton exchange membrane fuel cell grid-connected system based on resonant current controller," *International Journal of Hydrogen Energy*, Vol. 39, No. 26, pp. 14402-14410, Sep. 2014.

[12] M. G. Molina and P. E. Mercado, "Power flow stabilization and control of microgrid with wind generation by superconducting magnetic energy storage," *IEEE Trans. Power Electron.*, Vol. 26, No. 3, pp. 910-922, Dec. 2011.

[13] T. Asao, R. Takahashi, and T. Murata, "Evaluation method of power rating and energy capacity of Superconducting Magnetic Energy Storage system for output smoothing control of wind farm," *ICEM 2008. 18th International Conference on Electrical Machines*, pp. 1-6, 2008.

[14] M. G. Molina and P. E. Mercado, "Power flow control of microgrid with wind generation using a DSTATCOM-UCES," *IEEE International Conference on Industrial Technology (ICIT)*, pp. 955-960, 2010.

[15] I. Hadipaschalis, A. Poullikkas, and V. Efthimiou, "Overview of current and future energy storage technologies for electric power applications," *Renewable Sustainable Energy Rev.*, Vol. 13, No. 6-7, pp. 1513-1522, Aug./Sep. 2009.

[16] A. S. Subburaj, B. N. Pushpakaran, and S. B. Bayne, "Overview of grid connected renewable energy based battery projects in USA," *Renewable and Sustainable Energy Reviews*, Vol. 45, pp. 219-234, May 2015.

[17] Balijepalli, V. S. K. M, Pradhan, and V. Khaparde, "Review of demand response under smart grid paradigm," *Innovative Smart Grid Technologies - India (ISGT India), 2011 IEEE PES*, pp. 236-243, Dec. 2011.

[18] P. Kienzle and G. Andersson, "Valuing investments in multi-energy conversion, storage, and demand-side management systems under uncertainty," *IEEE Trans. Sustain. Energy*, Vol. 2, No. 2, pp. 194-202, Jan. 2011.

[19] C. Zhao and Topcu, "Optimal load control via frequency measurement and neighborhood area communication," *IEEE Trans. Power Syst.*, Vol. 28, No. 4, pp. 3576-3587, May 2013.

[20] M. Shankar, J. Nutaro, and J. Stovall, "Evolution of communication and control for electric grid load management," *IEEE Power and Energy Society General Meeting*, pp. 1-7, Jul. 2010.

[21] C. K. Lee, B. Chaudhuri, and S. Y. Hui, "Hardware and control implementation of electric springs for stabilizing future smart grid with intermittent renewable energy sources," *IEEE J. Emerg. Sel. Topics Power Electron.*, Vol. 1, No. 1, pp. 18-27, May 2013.

[22] C. K. Lee, K. L. Cheng, and W. M. Ng, "Load characterization of electric spring," *IEEE Energy Conversion Congress and Exposition (ECCE)*, pp. 4665-4670, Sep. 2013.

[23] C. K. Lee, S. C. Tan, and F. F. Wu, "Use of Hooke's law for stabilizing future smart grid– the electric spring concept," *IEEE Energy Conversion Congress and Exposition (ECCE)*, pp. 5253-5257, Sep. 2013.

[24] J. Soni, K. R. Krishnanand, and S. K. Panda, "Load-side demand management in buildings using controlled electric springs," *Industrial Electronics Society, IECON 2014 - 40th Annual Conference of the IEEE*, pp. 5376-5381, 2014.

[25] C. K. Lee and S. Y. Hui, "Reduction of energy storage requirements in future smart grid using electric springs," *IEEE Trans. Smart Grid*, Vol. 4, No. 3, pp. 1282-1288, Apr. 2013.

[26] C. K. Lee, N. R. Chaudhuri, and B.Chaudhuri, "Droop control of distributed electric springs for stabilizing future power grid," *IEEE Trans. Smart Grid*, Vol. 4, No. 3, pp. 1558-1566, Jul. 2015.

[27] Y. Shuo, S. C. Tan, and C. K. Lee, "Electric spring for power quality improvement," *2014 IEEE Applied Power Electronics Conference and Exposition - APEC 2014*, pp. 2140-2147, 2014.

[28] X. Che, T. Wei, and Q. Huo, "A general comparative analysis of static synchronous compensator and electric spring," *2014 IEEE Conference and Expo on Transportation Electrification Asia-Pacific (ITEC Asia-Pacific)*, pp. 1-5, 2014.

[29] X. Luo, Z. Akhtar, and C. K. Lee, "Distributed voltage control with electric springs: comparison with STATCOM," *IEEE Trans. Smart Grid*, Vol. 6, No. 1, pp. 209-219, Aug. 2014.

[30] R. Kabiri, G. Holmes, and B. McGrath, "LV grid voltage regulation using transformer electronic tap changing, with

PV inverter reactive power injection," *IEEE J. Emerg. Sel. Topics Power Electron.*, Vol. 3, No. 4, pp. 1182-1192, Jun. 2015.
[31] C. R. Fuerte-Esquivel, E. Acha, and I. Ambriz-Perez, "Integrated SVC and step-down transformer model for Newton-Raphson load flow studies," *IEEE Power Eng. Rev.*, Vol. 20, No. 2, pp. 45-46, Feb. 2000.
[32] P. Melato, N. Mbuli, and J. Pretorius, "Serving low load levels by derating line voltage using step down transformers," *50th International Universities Power Engineering Conference (UPEC)*, pp. 1-5, 2015.
[33] R. Majumder, A. Ghosh, and G. Ledwich, "Power management and power flow control with back-to-back converters in a utility connected microgrid," *IEEE Trans. Power Syst.*, Vol. 25, No. 2, pp. 821-834, Nov. 2009.
[34] E. Martinez, I. Fernandez, and J. Canales, "Thyristor based solid state tap changer for distribution transformers," 2013 IEEE 11th International Workshop of Electronics, Control, Measurement, Signals and their application to Mechatronics (ECMSM), pp. 1-5, Jun. 2013.
[35] S. M. Garcia, J. Rodriguez, and J. Antonio, "Feasibility of electronic tap-changing stabilizers for medium voltage lines – Precedents and new configurations," *IEEE Trans. Power Del.*, Vol. 24, No. 3, pp. 1490-1503, Jun. 2009.
[36] H. Jiang, R. Shuttleworth, and B. Zahawi, "Fast response GTO assisted novel tap changer," *IEEE Trans. Power Del.*, Vol. 16, No. 1, pp. 111-115, Jan. 2001.
[37] J. Faiz and B. Siahkolah, "New solid-state onload tap-changers topology for distribution transformers," *IEEE Trans. Power Del.*, Vol. 18, No. 1, pp. 136-141, Jan. 2003.
[38] J. Faiz and B. Siahkolah, "Optimal configurations for taps of windings and power electronic switches in electronic tap-changers," *IEE Proceedings - Generation, Transmission and Distribution*, Vol. 149, No. 5, pp. 517-524, Dec. 2002.
[39] S. Bhowmik and R. Spee, "A guide to the application-oriented selection of AC/AC converter topologies," *IEEE Trans. Power Electron.*, Vol. 8, No. 2, pp. 156-163, Feb. 1993.
[40] C. Wang and C. Su, "A Novel Common-Neutral Single-Stage Single-Phase AC/DC/AC Converter with High Input Power Factor," *37th IEEE Power Electronics Specialists Conference, 2006. PESC '06*, pp. 1-5, 2006.
[41] The MathWorks Inc., SimPowerSystems™ *R2013b User's Guide (Second Generation)*, 2013.
[42] N. Vazquez, A. Velazquez, and C. Hernandez, "AC voltage regulator based on the AC-AC buck-boost converter," *IEEE International Symposium on Industrial Electronics*, pp. 533 - 537, Jun. 2007.
[43] IEEE Standard 141-1993.
[44] IEEE Standard 519-1992.
[45] W. Wangdee, "Reliability Impact of intermittent renewable energy source integration into power system," *2014 IEEE International Electrical Engineering Congress (iEECON)*, pp. 1-4, 2014

Kun Liu was born in Jiangxi, China. He received his B.S. degree in Electrical Engineering from Shanghai Jiao Tong University, Shanghai, China, in 2014, where he is presently working towards his M.S. degree in Electrical Engineering with a specialization in Power Electronics. His current research interests include DC-DC converters, contactless inductive power transfer, as well as the control and stability of microgrids and smart grids.

Muhammad Mansoor Khan was born in Lahore, Pakistan. He received his B.S. degree in Electronics from the NED University of Engineering and Technology, Karachi, Pakistan; his M.S. degree in System Engineering from Quaid-i-Azam University, Islamabad, Pakistan; and his Ph.D. degree from Shanghai Jiao Tong University, Shanghai, China, in 2002. He has been with the Department of Electrical Engineering for past 12 years, and is presently serving as an Associate Professor. He has coauthored more than 30 SCI papers. His current research interests include power electronic converters, power quality equipment, solar inverters, solid-state transformers, as well as the control and stability of microgrids and smart grids.

Ahmad Rana received his B.S. degree in Electrical Engineering (with honors) from the University of Engineering and Technology, Lahore, Pakistan; his M.S. degree in Systems Engineering with a specialization in Nuclear Instrumentation and Control from the Center for Nuclear Studies, Nilore, Pakistan; and his Ph.D. degree in Robotics from the University of Sheffield, Sheffield, ENG, UK. He is actively involved in applied research, and is a Research Associate at the Villanova Center for Analytics of Dynamic Systems of Villanova University, Villanova, PA, USA. He also runs a consultant firm offering services in industrial control. His current research interests include embedded control systems for power electronics, and telecommunication systems for distributed embedded control.

Dong Fei received his B.S. degree in Mechanical Engineering from Tongji University, Shanghai, China, in 2005; and his M.S. degree in Electrical Engineering from Shanghai Jiao Tong University, Shanghai, China, in 2012. From 2005 to 2010, he was with the State Grid Shanghai Municipal Electric Power Company, Shanghai, China. In 2010, he joined State Grid Shanghai Procurement Company, Shanghai, China. His current research interests include DC-DC converters, and PWM converter/inverter systems.